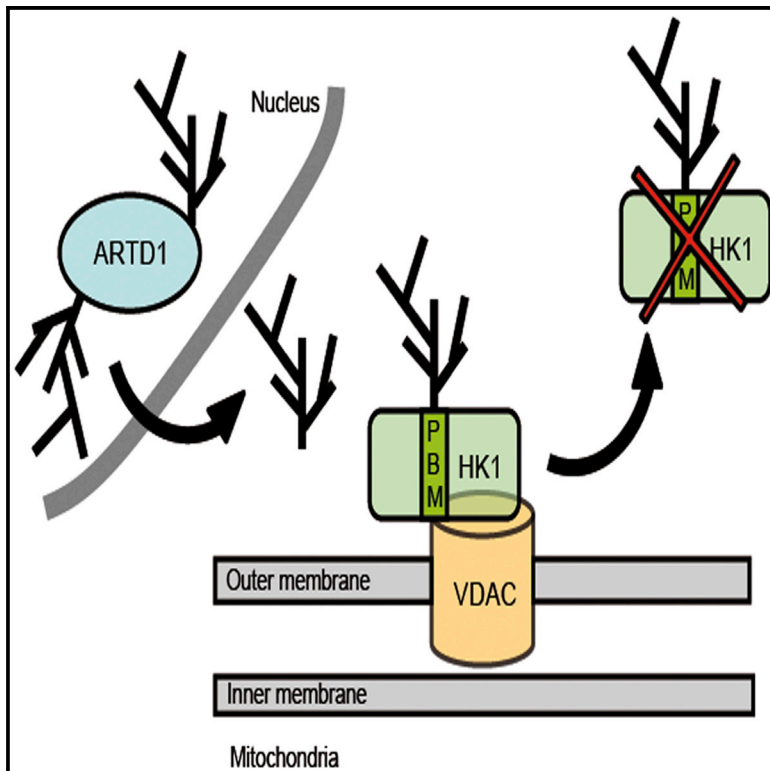


ARTD1/PARP1 Negatively Regulates Glycolysis by Inhibiting Hexokinase 1 Independent of NAD⁺ Depletion

Graphical Abstract



Authors

Elise Fouquerel, Eva M. Goellner, ..., Guy G. Poirier, Robert W. Sobol

Correspondence

rws9@pitt.edu

In Brief

ARTD1-induced cell death is associated with NAD⁺ depletion and ATP loss, but the molecular mechanism of ARTD1-mediated energy collapse remains elusive. Fouquerel et al. show that ARTD1-mediated PAR synthesis, but not direct NAD⁺ depletion, blocks glycolysis and leads to ATP loss. These findings support a working model in which ARTD1 hyperactivation leads to inhibition and mislocalization of hexokinase-1, causing reduced glycolysis and depletion of cellular ATP pools.

Highlights

ARTD1 activation-mediated ATP depletion initiates in the mitochondria

ARTD1 activation suppresses glycolysis and oxidative phosphorylation

NAD⁺ depletion does not affect glycolysis or cellular ATP levels

HK1 activity is inhibited by ARTD1 activation to suppress glycolysis



ARTD1/PARP1 Negatively Regulates Glycolysis by Inhibiting Hexokinase 1 Independent of NAD⁺ Depletion

Elise Fouquerel,^{1,2,7} Eva M. Goellner,^{1,2,7,8} Zhongxun Yu,^{2,3} Jean-Philippe Gagné,⁴ Michelle Barbi de Moura,^{1,2} Tim Feinstein,¹ David Wheeler,¹ Philip Redpath,⁵ Jianfeng Li,^{1,2} Guillermo Romero,¹ Marie Migaud,⁵ Bennett Van Houten,^{1,2} Guy G. Poirier,⁴ and Robert W. Sobol^{1,2,6,*}

¹Department of Pharmacology & Chemical Biology, University of Pittsburgh School of Medicine, Pittsburgh, PA 15213, USA

²University of Pittsburgh Cancer Institute, Hillman Cancer Center, Pittsburgh, PA 15213, USA

³School of Medicine, Tsinghua University, No.1 Tsinghua Yuan, Haidian District, Beijing 100084, China

⁴Centre de recherche du CHU de Québec, Université Laval, Faculté de Médecine, Québec, Canada

⁵School of Pharmacy, Queen's University, Belfast BT9 7BL, UK

⁶Department of Human Genetics, University of Pittsburgh Graduate School of Public Health, Pittsburgh, PA 15213, USA

⁷Co-first author

⁸Present address: Ludwig Institute for Cancer Research, University of California School of Medicine San Diego, 9500 Gilman Drive, La Jolla, CA 92093-0669, USA

*Correspondence: rws9@pitt.edu

<http://dx.doi.org/10.1016/j.celrep.2014.08.036>

This is an open access article under the CC BY-NC-ND license (<http://creativecommons.org/licenses/by-nc-nd/3.0/>).

SUMMARY

ARTD1 (PARP1) is a key enzyme involved in DNA repair through the synthesis of poly(ADP-ribose) (PAR) in response to strand breaks, and it plays an important role in cell death following excessive DNA damage. ARTD1-induced cell death is associated with NAD⁺ depletion and ATP loss; however, the molecular mechanism of ARTD1-mediated energy collapse remains elusive. Using real-time metabolic measurements, we compared the effects of ARTD1 activation and direct NAD⁺ depletion. We found that ARTD1-mediated PAR synthesis, but not direct NAD⁺ depletion, resulted in a block to glycolysis and ATP loss. We then established a proteomics-based PAR interactome after DNA damage and identified hexokinase 1 (HK1) as a PAR binding protein. HK1 activity is suppressed following nuclear ARTD1 activation and binding by PAR. These findings help explain how prolonged activation of ARTD1 triggers energy collapse and cell death, revealing insight into the importance of nucleus-to-mitochondria communication via ARTD1 activation.

INTRODUCTION

The human genome encodes 17 poly(ADP-ribose) polymerase (PARP) or ADP-ribosyltransferase diphtheria toxin-like (ARTD) proteins that are involved in regulating a variety of cellular processes including DNA damage signaling and repair, chromatin remodeling, transcription, epigenetic gene regulation, mitosis, and differentiation (Hassa et al., 2006). All of the catalytically active members of the ARTD/PARP family consume NAD⁺ to

catalyze ADP-ribosylation of their target substrates but are classified as mono- or poly-(ADP-ribosyl) transferases depending on their ability to transfer monomers or polymers of ADP-ribose (Hottiger et al., 2010). In particular, poly(ADP-ribosylation) is known for its switch-like effects on acceptor proteins by virtue of its high charge density and steric hindrance. As a consequence, this posttranslational modification can activate or inhibit protein functions, disrupt or promote protein-protein interactions, or facilitate protein subcellular relocalization (Hottiger et al., 2010).

ADP-ribosyltransferase diphtheria toxin-like 1 (ARTD1 or PARP1) primarily functions as a key enzyme of the base excision repair (BER) and single-strand break repair (SSBR) pathways (Almeida and Sobol, 2007). ARTD1 participates in additional DNA repair pathways such as nonhomologous end-joining (NHEJ), nucleotide excision repair (NER), in sensing and repairing DNA double-strand breaks and is suggested to participate in the excision step during mismatch repair (De Vos et al., 2012). The participation of ARTD1 in these DNA repair pathways depends on its ability to detect and bind to DNA single-strand breaks with high affinity (Langelier et al., 2012). In BER, a strand break is a normal repair intermediate, which is formed following hydrolysis of the DNA backbone by an apurinic/apyrimidinic endonuclease, APE1 (Almeida and Sobol, 2007; Svilar et al., 2011), triggering ARTD1 activation. Upon activation, ARTD1 synthesizes poly-(ADP-ribose) (PAR) that functions as a mechanism of chromatin decondensation and generates a loading platform for the recruitment of the BER machinery to the lesion site, including proteins such as X-ray repair complementing defective repair in Chinese hamster cells 1 (XRCC1), poly (ADP-ribose) glycohydrolase (PARG) and DNA polymerase β (Pol β ; Schreiber et al., 2006; Svilar et al., 2011). Successful recruitment of the downstream BER proteins facilitates repair of the strand break, suppressing further ARTD1 activity and PAR synthesis (Masson et al., 1998; Tang et al., 2010).

Conversely, unrepaired DNA breaks, resulting from excessive genotoxin exposure and/or from DNA repair defects, leads to persistent ARTD1 activation and cell death (Gottipati et al., 2010; Juarez-Salinas et al., 1979; Tang et al., 2010). Uncontrolled or excessive activation of ARTD1 is responsible for numerous pathological outcomes including streptozotocin-induced pancreatic beta-cell death and the onset of diabetes (Burns and Gold, 2007; Masutani et al., 1999; Pieper et al., 1999) as well as tissue injury from cerebral and myocardial ischemia (Eliasson et al., 1997; Endres et al., 1997; Pieper et al., 2000). In these and other mouse model studies, ARTD1 activation-induced tissue injury results from the accumulation of DNA repair intermediates (Calvo et al., 2013).

Cell death due to ARTD1 activation was originally suggested to involve energy metabolite (NAD^+ and ATP) depletion (Berger, 1985; Berger et al., 1983; Jacobson et al., 1980). However, the molecular mechanisms underlying ARTD1 hyperactivation-induced ATP depletion and the resulting cell death are unresolved. Confounding this issue, cell type and in particular cellular proliferation status, has yielded widely disparate observations. In astrocytes, cytosolic NAD^+ depletion resulting from ARTD1 activation is suggested to trigger a glycolytic block that can be rescued by NAD^+ or tricarboxylic acid (TCA) cycle substrates, such as α -ketoglutarate and pyruvate (Ying et al., 2002, 2003). Neuronal cell death from ARTD1 activation is triggered by unregulated PAR synthesis, termed parthanatos (Andrabi et al., 2008) and has been suggested to play a role in multiple experimental and physiopathological scenarios, including stroke, diabetes, inflammation, and neurodegeneration. Some reports demonstrate a direct link between ARTD1 hyperactivation and mitochondrial dysfunction, notably through the loss of NAD^+ that precedes the induction of the mitochondrial depolarization and mitochondria outer membrane permeability transition (Alano et al., 2004; Cipriani et al., 2005). In contrast, in apoptosis-deficient cells, it is suggested that only cells relying on glycolysis are sensitive to DNA damage-mediated ARTD1 hyperactivation and necrotic cell death (Zong et al., 2004).

Herein, we tested the hypothesis that the glycolytic block and loss of ATP induced by DNA damage-induced ARTD1 activation is distinct from the resulting loss of NAD^+ . In addition, we demonstrate that ARTD1 activation and the resulting synthesis of PAR facilitates the block to glycolysis via regulation/inhibition of PAR binding proteins including the essential glycolytic enzyme hexokinase 1 (HK1).

RESULTS

ARTD1 Activation Induced by DNA Repair Intermediates Triggers Energy Metabolite Depletion in Glioblastoma Cells

The acute cellular response to DNA alkylation damage is dependent on the expression of the methyl-specific DNA glycosylase MPG (also known as AAG or ANPG; Tang et al., 2010) and an imbalance in BER protein expression can lead to an accumulation of toxic DNA repair intermediates (Fu et al., 2012). To evaluate the cellular consequences of DNA damage-induced DNA repair intermediates, we used a glioblastoma-derived cell line, LN428, with low levels of MPG and the isogenic derivative

LN428/MPG overexpressing MPG (Figures S1A–S1D available online).

Upon activation, ARTD1 transfers the ADP-ribosyl unit of NAD^+ to synthesize PAR and as a consequence, leads to the rapid loss of total cellular NAD^+ . ARTD1 activation also leads to the concomitant loss of ATP and the onset of necrosis (Ha and Snyder, 1999; Tang et al., 2010). Exposure of LN428/MPG cells to MNNG (5 μM) results in the loss of close to 90% and 70% respectively, of total cellular NAD^+ and ATP pools with no measurable metabolite depletion observed in the control LN428 cells at this dose of MNNG (Figures 1A and 1B). As expected, pretreatment with the PARP-inhibitors ABT-888 or BMN-673 significantly rescues the MNNG-induced NAD^+ loss in the LN428/MPG cells (Figure 1C). Importantly, ARTD1 inhibition completely attenuates the MNNG-induced loss of ATP in LN428/MPG cells (Figures 1D and S1K). To further investigate the involvement of ARTD1 in NAD^+ and ATP loss, we depleted ARTD1 expression using an shRNA coupled with overexpressed MPG via viral transduction of LN428 cells, as described in the Supplemental Experimental Procedures. We verified ARTD1 knockdown and MPG overexpression by RT-PCR and immunoblot (Figures S1G and S1H). PAR synthesis in LN428/ARTD1-KD/MPG cells is largely impaired (Figure S1H) after MNNG even at 10 μM , as compared to LN428/MPG cells (Figure S1D). Importantly, LN428/ARTD1-KD/MPG cells present no defect in NAD^+ nor ATP levels following MNNG treatment, demonstrating a direct role for ARTD1 in the loss of energy metabolites (Figures 1C and 1D; gray bars).

Real-Time Analysis of ATP Levels in Glioblastoma Cells: ARTD1 Activation-Mediated ATP Depletion Initiates in the Mitochondria

ATP is generated in both the cytosol and the mitochondria via glycolysis and oxidative phosphorylation, respectively. However, classical measurements of ATP levels lack subcellular specificity, limiting the conclusions that can be drawn. To monitor changes in ATP levels in different compartments of living cells as a function of MNNG exposure, LN428 and LN428/MPG cells were transiently transfected with FRET-based ATP sensors, specifically targeted to the mitochondria (AT1.03m), cytosol (AT1.03c), or nucleus (AT1.03n), which produce a YFP FRET signal upon ATP binding (Imamura et al., 2009b). An increase of the CFP/YFP ratio therefore indicates a loss of ATP bound to the FRET sensor. Expression of the FRET-based ATP sensors showed the expected subcellular localization measured 48 hr post-transfection (Figure S1I) and localization was not affected by DNA damaging agent or PARP inhibitor treatment (not shown).

For both the LN428 and LN428/MPG cells, a 10-minute baseline FRET ratio was determined prior to the addition of MNNG (5 μM). A low CFP/YFP ratio was observed prior to treatment suggesting normal baseline ATP levels in all subcellular compartments, consistent with whole cell metabolite measurements (Figure 1B). The different subcellular compartments had slight differences in the absolute starting CFP/YFP ratio and were normalized to 1 at the baseline to compare changes between compartments (Figure S1J). Consistent with the whole cell ATP analysis, the CFP/YFP ratio remains close to the baseline in all three subcellular compartments for up to 60 min after MNNG exposure of the LN428 cells (Figure 1E), indicating that any changes in subcellular

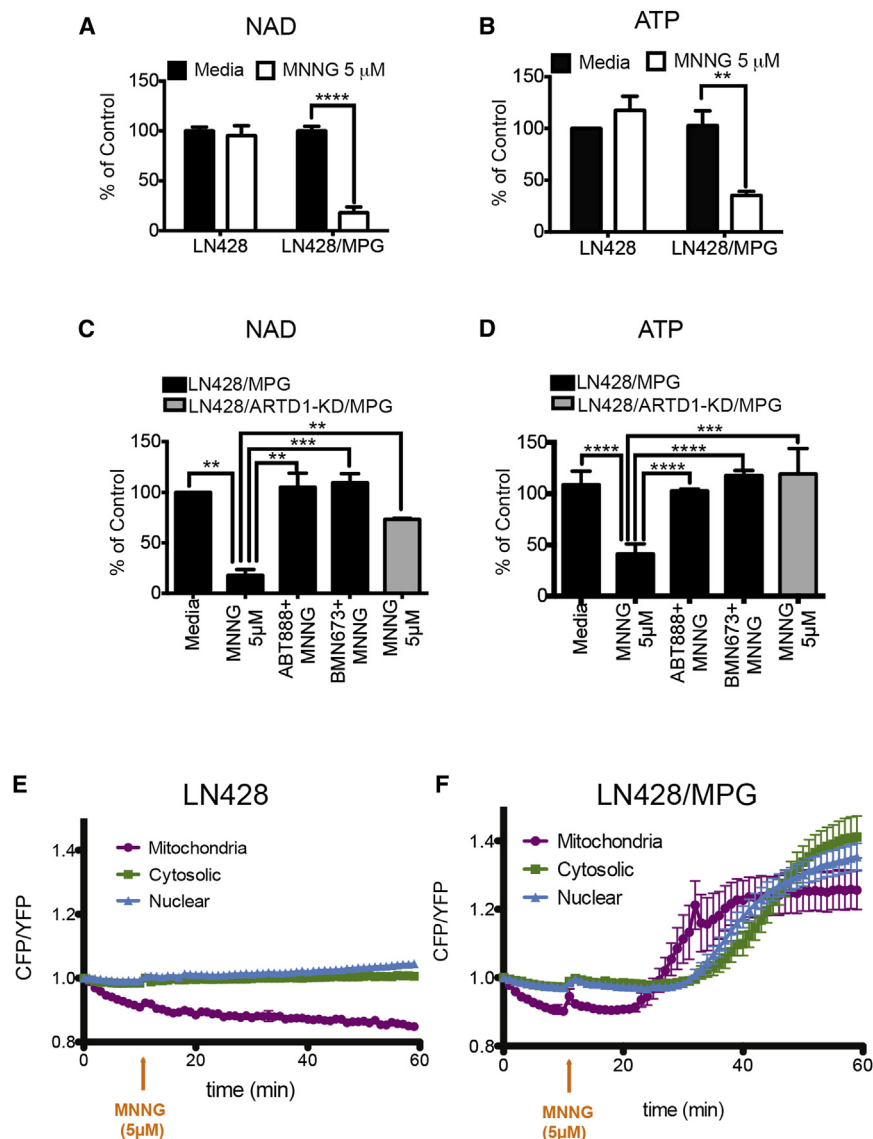


Figure 1. ARTD1 Hyperactivation Induced by DNA Repair Intermediates Triggers Energetic Depletion in Glioblastoma Cells

(A and B) Global NAD⁺ (A) and global ATP (B) levels in LN428 and LN428/MPG cells after 1hr treatment with either media or 5 μ M MNNG. The data shown is the average of 3 independent experiments \pm SD and are reported as percentage of the untreated control cell line (LN428): (A) ****p < 0.0001 (B) **p = 0.01.

(C and D) Global NAD⁺ (C) and global ATP (D) levels in LN428/MPG cells (black bars) or in LN428/ARTD1-KD/MPG cells (gray bar) after a 1hr treatment with either media, 5 μ M MNNG or 5 μ M MNNG after a pretreatment with ARTD1 inhibitors ABT-888 or BMN673, as indicated. The data shown is the average of three independent experiments \pm SD and are reported as percentage of the untreated cells: (C) **p < 0.005, ***p = 0.0003, (D) ****p < 0.0001, ***p < 0.001.

(E and F) FRET ratio calculated in the compartments of LN428 cells (E) or LN428/MPG cells (F) transfected with the indicated FRET sensors. Images were acquired each minute. A ten-minute baseline period was recorded before cells were treated with 5 μ M MNNG (orange arrow). FRET traces shown are the mean of five to seven cells (LN428) or seven to nine (LN428/MPG) \pm SE.

ATP due to the minimal PAR formation must be below the sensitivity of the FRET sensors. However, exposure of the LN428/MPG cells to MNNG results in a rapid and dramatic change in the CFP/YFP ratio, in line with the observed loss of total cellular ATP (Figures 1B and 1F) (see Movies S1–S3). Surprisingly, of the three subcellular compartments, an increase in the CFP/YFP ratio (and hence a loss of ATP) was first observed in the mitochondria. The MNNG-induced loss of ATP in the mitochondria began 12 min after the start of MNNG treatment, concomitant with the peak of PAR production (Figures 1F and S1D) followed by a decrease in both the cytosolic and nuclear ATP pools, beginning 24 min after MNNG exposure (Figures 1F and S1I). In the whole cell ATP analysis, the MNNG-induced loss of ATP in the LN428/MPG cells was completely blocked when ARTD1 was inhibited or depleted (Figure 1D). Similarly, pretreatment of LN428/MPG cells with the PARP inhibitor was able to rescue the ATP loss in all three subcellular compartments (Figures S1K and S1L). These results

support an ARTD1-dependent signal that provides a means of intracellular communication between the nucleus and the mitochondria in response to genotoxic stress.

Nuclear to Mitochondrial Communication via ARTD1 Activation: DNA Damage-Induced Defects in Glycolysis and Oxidative Phosphorylation

It has been hypothesized that NAD⁺ consumption by ARTD1 activation is causa-

tive for the rapid depletion of cellular ATP. The kinetics of loss of the mitochondrial, cytosolic, and nuclear ATP pools in response to ARTD1 activation suggests that variations in the total cellular level of NAD⁺ may signal from the nucleus to the mitochondria by regulating NAD⁺-dependent enzymes critical for ATP biosynthesis. To examine this, we measured multiple parameters of glycolysis and mitochondrial oxidative phosphorylation in live-cell conditions with the Seahorse XF24 extracellular flux analyzer (SEFA), essentially as described (Qian and Van Houten, 2010; Varum et al., 2011). This real-time, live-cell analysis allows a measure of DNA damage-dependent changes in oxidative phosphorylation (oxygen consumption rate, OCR) and glycolysis (extracellular acidification rate, ECAR). The sequential addition of four metabolic inhibitors: oligomycin, FCCP, 2-deoxyglucose, and rotenone allows the calculation of four critical metabolic parameters: (1) the ATP-coupled OCR; (2) the total mitochondrial reserve capacity (TRC), or maximal

respiratory rate; (3) the basal ECAR, which corresponds to the basal glycolytic rate; and (4) the oligomycin-induced ECAR.

As expected, the isogenic LN428 and LN428/MPG cell lines have similar basal ECAR and OCR profiles (Figures 2A and 2B; left), ideal for comparative analysis. Changes in glycolysis and oxidative phosphorylation were then measured in response to MNNG (1 hr, 5 μ M) and in combination with ARTD1 knockdown or inhibition by pretreatment with either ABT-888 or BMN-673. In line with earlier reports using mouse astrocytes (Berger, 1985; Ying et al., 2003), strong ARTD1 activation resulted in the complete loss of glycolysis after MNNG treatment, leading to a decrease of both basal and induced ECAR in LN428/MPG but not in LN428 cells (Figures 2A and S2A). Consistent with our hypothesis that the metabolic defects result from ARTD1 activation, ABT-888 or BMN-673 treatment prior to MNNG exposure leads to a complete rescue of both basal and induced ECAR in LN428/MPG cells (Figures 2C and S2A). Moreover, we show that exposure of LN428/ARTD1-KD/MPG cells to MNNG does not lead to a loss of glycolytic rate as seen in the LN428/MPG cells (Figures 2F and S2D), providing further evidence for the direct involvement of ARTD1 in this defect of cellular metabolism.

Consistent with the observed loss of NAD⁺ and ATP in the LN428/MPG cells in response to MNNG, we found that these cells undergo a complete loss of TRC, with no change to the ATP-coupled OCR (Figure 2B; right). The LN428 cells also present with a partial yet significant loss (50%) of TRC in response to MNNG treatment. To determine if the effects observed in both cell lines was the sole result of ARTD1 activation and NAD⁺ depletion, the identical analysis was performed with ARTD1 inhibited by pretreatment with ABT-888 or BMN-673. Interestingly, we observed a complete rescue of TRC in LN428 cells upon ARTD1 inhibition (Figures 2E and S2C). These data suggest that even a low level of ARTD1 activation (in the case of LN428 cells and illustrated by the anti-PAR immunoblot; Figure S1D) is able to affect the mitochondrial reserve capacity. ARTD1 inhibition is also able to rescue the mitochondrial reserve capacity defect of MNNG-treated LN428/MPG cells (Figures 2D and S2B). To further investigate the role of ARTD1 in MNNG-induced OCR defects, we submitted LN428/ARTD1-KD and LN428/ARTD1-KD/MPG cells to the same treatment and performed the same analysis. As expected, we show that LN428/ARTD1-KD cells do not present the partial defect observed in LN428 cells after MNNG treatment. Expressing MPG in the LN428/ARTD1-KD cells (LN428/ARTD1-KD/MPG) does not trigger a loss of TRC in response to MNNG treatment such as that seen in the LN428/MPG cells (Figure 2G). These results strongly suggest that cellular oxidative phosphorylation, as measured by oxidative reserve capacity, is extremely sensitive to ARTD1 activation. The same results have been observed in HeLa cells treated with increasing doses of MNNG, demonstrating that the MNNG induced metabolic defects are not glioblastoma specific nor an artifact of MPG overexpression, but applicable to multiple cell types (Figures S2F–S2J). From these data, we hypothesize that ARTD1 activation acts as the initiating signal from the nucleus to mediate suppression of both glycolytic and mitochondrial oxidative phosphorylation activity.

NAD⁺ Depletion Is Not Sufficient to Decrease Glycolysis or Cellular ATP Levels

One of the strongest phenotypes associated with ARTD1 activation is an acute loss of NAD⁺, with 90% of the cellular NAD⁺ content lost within 1 hour (Figure 1A). Therefore, a likely candidate to signal ARTD1 activation in the nucleus to the metabolic machinery in the mitochondria is the change in overall NAD⁺ content. To test this hypothesis, we directly reduced NAD⁺ levels in the absence of ARTD1 activation. To inhibit NAD⁺ biosynthesis, LN428/MPG cells were treated with FK866, a selective small molecule inhibitor of the essential NAD⁺ biosynthesis enzyme nicotinamide phosphoribosyltransferase (NAMPT; Figure 3A; Hasmann and Schemainda, 2003). After a 24 hr treatment with FK866 (10 nM), the NAD⁺ pool decreased by approximately 75%, roughly equivalent to the NAD⁺ loss after ARTD1 activation (Figure 3B). Surprisingly, however, ATP levels remained constant and viability was not affected in LN428/MPG cells after treatment with FK866 (Figures 3C and S3A).

Consistent with a role for NAD⁺ as a cofactor in mitochondrial enzymatic reactions, FK866-treated cells displayed a significant decrease in total mitochondrial reserve capacity (Figures 3D and S3B). Surprisingly, NAD⁺ depletion by FK866 treatment had no effect on either the basal or induced ECAR, unlike MNNG treatment (Figures 3E and S3C). To demonstrate specificity and selectivity of FK866, treated cells were also supplemented with nicotinamide riboside (NR), a precursor that does not require NAMPT for conversion to NAD⁺ (Figure 3A). NR was synthesized and purified as described in the Supplemental Experimental Procedures (Figure S4). As expected, NR pretreatment could overcome the NAD⁺ depletion induced by FK866 (Figure 3F); however, NR did not prevent the loss of NAD⁺ or ATP after MNNG even at a 10-fold higher dose (Figures 3F and 3G). Consistently, the FK866-induced loss of TRC is completely rescued by NR (Figures 3H and S3D) but NR was unable to rescue the OCR and ECAR defects in LN428/MPG cells treated with MNNG (Figures 3H, 3I, S3D, and S3E). Yet, at low doses of MNNG, NR pretreatment was able to partially rescue NAD⁺ levels (Figure S3F). Interestingly, this partial rescue was not sufficient to overcome the OCR and ECAR defects (Figures S3G and S3H), suggesting a more complex effect of ARTD1 activation on cellular metabolism. The sensitivity of oxidative phosphorylation but not glycolysis to direct depletion of NAD⁺, suggests that ARTD1-mediated consumption of NAD⁺ is a major contributor to the DNA damage-induced loss of oxidative phosphorylation, but inhibition of glycolysis occurs through another unknown mechanism of ARTD1 activation.

PARG Knockdown Rescues the Glycolytic Defect in MNNG-Treated Cells

The nucleo-cytoplasmic translocation of PAR has been extensively described (Andrabi et al., 2006). As an example, it has been demonstrated that the movement of PAR into the cytosol triggers the release of the mitochondrial protein AIF upon binding of PAR to the AIF PAR-binding motif (PBM; Yu et al., 2006). This phenomenon has recently been shown to require the endo- and exoglycohydrolase activities of PARG (Mashimo et al., 2013; Wang et al., 2011; Yu et al., 2002). To investigate whether the glycolytic defects observed herein are due to a release of PAR

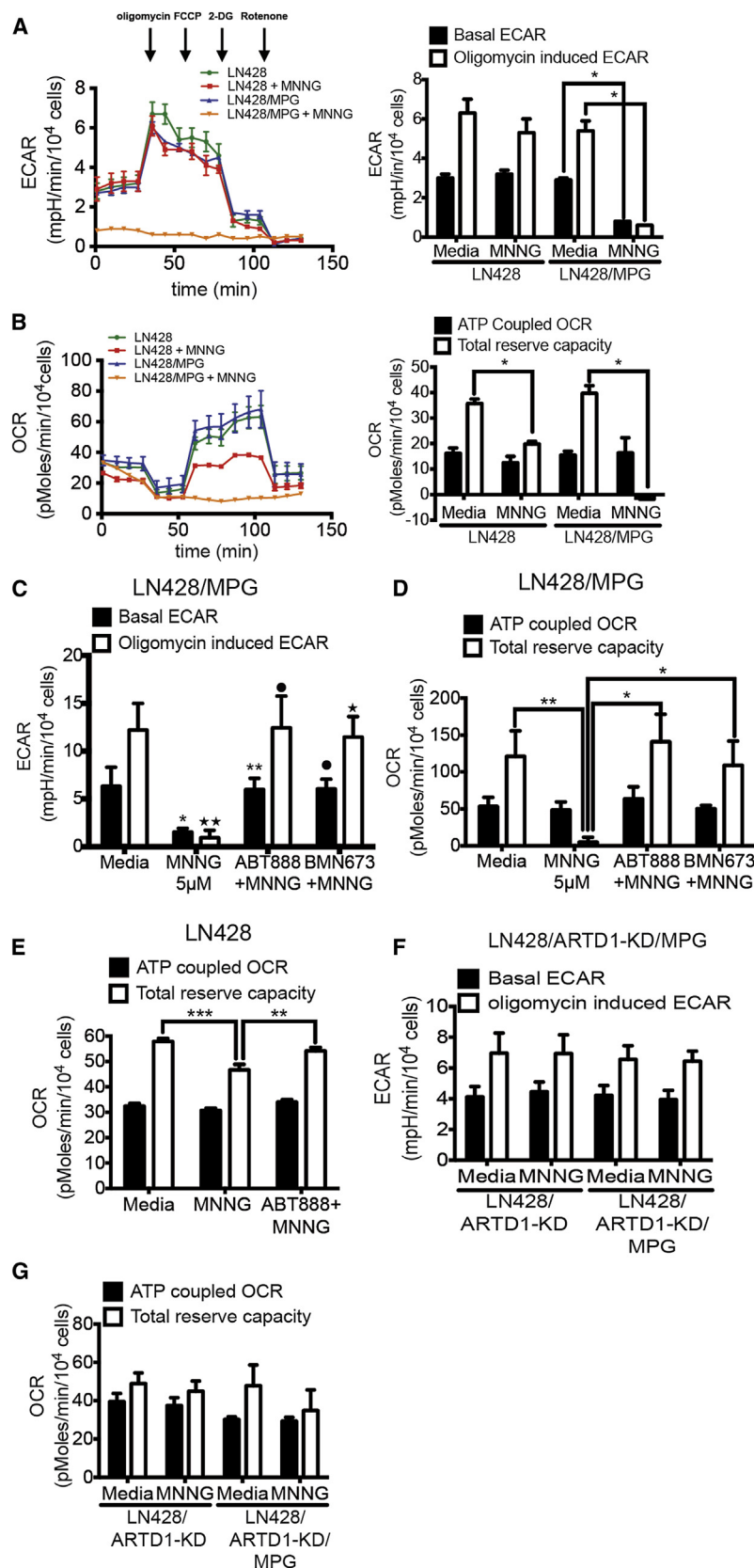


Figure 2. Mitochondrial Dysfunction following Alkylating Agent-Induced ARTD1 Activation

(A and B) Seahorse extracellular flux analyzer (SEFA) measurement of ECAR metabolic profile (A) or OCR metabolic profile (B) in LN428 or LN428/MPG cells treated with either media or MNNG (5 μ M, 1 hr). Bar graphs representing basal ECAR and oligomycin induced ECAR (A) or ATP coupled OCR and total reserve capacity (TRC) (B) are shown on the right. Traces shown are the mean of two independent experiments in which each data point represents technical replicates of five wells each \pm SE. Basal and induced ECAR rates, ATP coupled OCR and TRC are calculated using the average of 3 data points collected for each metabolic inhibitor, \pm SD ($*p < 0.05$).

(C and D) ECAR measurements (C) and OCR measurements (D) in LN428/MPG cells treated with 5 μ M MNNG following pretreatment with media control or ARTD1 inhibitors ABT-888 or BMN-673 as indicated. Shown is the mean of three independent experiments \pm SD as described above: (C) $*p < 0.05$ compared to media for basal ECAR, $\bullet p < 0.05$ compared to MNNG for basal ECAR, $**p < 0.005$ compared to media for induced ECAR, $\bullet p < 0.005$ compared to MNNG for induced ECAR, $*p < 0.01$ compared to MNNG for induced ECAR; (D) $*p < 0.05$, $**p < 0.01$.

(E) OCR measurement in LN428 cells treated with 5 μ M MNNG following pretreatment with media control or ARTD1 inhibitor ABT-888. Shown is the mean of three independent experiments \pm SD ($***p < 0.0004$ compared to media control for TRC, $**p < 0.002$ compared to MNNG for TRC).

(F and G) ECAR measurement (F) and OCR measurement (G) for LN428/ARTD1-KD or LN428/ARTD1-KD/MPG cells after treatment with media control or 5 μ M MNNG. Shown is the average of three independent experiments \pm SD as described above.

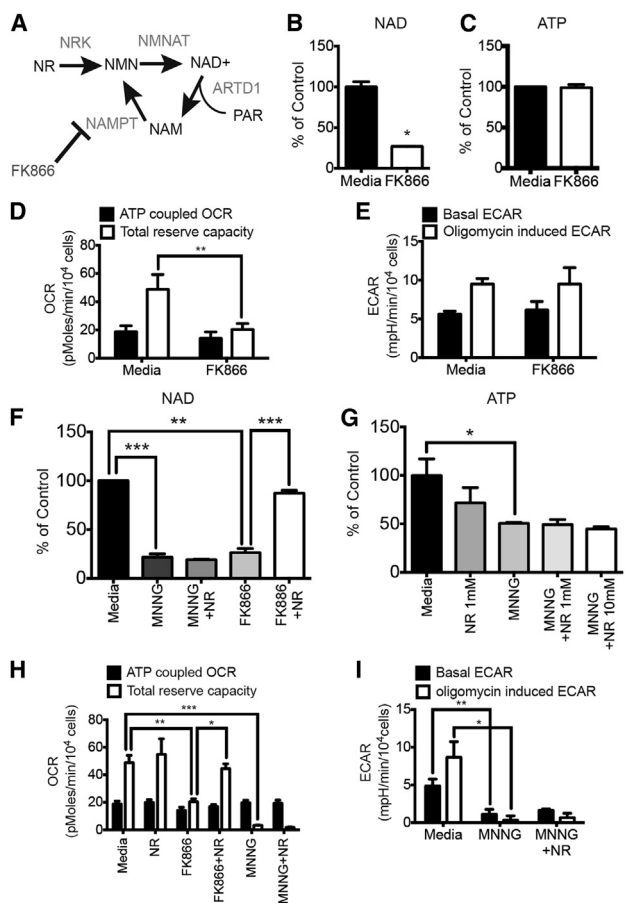


Figure 3. NAD⁺ Depletion Does Not Alter Glycolysis in LN428/MPG Cells

(A) Schematic of NAD⁺ biosynthesis from nicotinamide riboside (NR) and from recycling after ARTD1 consumption of NAD⁺-releasing nicotinamide (NAM). NAM is subsequently phosphorylated by nicotinamide phosphoribosyl transferase (NAMPT), an enzyme selectively inhibited by FK866.

(B and C) Global NAD⁺ (B) and global ATP (C) measurement in LN428/MPG cells after 24 hr of treatment with media or FK866 (10 nM). The data shown is the average of three independent experiments \pm SD and are reported as percentage of the untreated cells; (B)* p < 0.05.

(D) Seahorse measurement of the OCR metabolic profile was performed in LN428/MPG cells treated with either media control or FK866 (10 nM) for 24 hr. Shown is the mean of four independent experiments \pm SD (** p < 0.01).

(E) Seahorse measurement of the ECAR metabolic profile was performed as above. Shown is the mean of two independent experiments \pm SD.

(F) Global NAD⁺ level in LN428/MPG cells after either media, NR (1 mM) or FK866 (10 nM) with or without NR (1 mM) as a 24 hr pretreatment. Cells treated with MNNG, and pretreated or not by NR, are incubated 1 hr with MNNG prior the analysis (*** p < 0.0005, ** p < 0.001).

(G) Global ATP levels after 24 hr treatment with either media (black bar) or NR (1 mM; dark gray bar), or NR (10 mM) followed by media alone or media supplemented with MNNG (5 μ M, 1 hr; dark-gray, light-gray and white bars; * p < 0.05).

(H) OCR metabolic profile of LN428/MPG cells treated with either media control or NR (1 mM) and/or FK866 (10 nM) followed by media alone or media supplement with MNNG (5 μ M, 1 hr). Data are the mean of four independent experiments \pm SD (*** p < 0.005, ** p < 0.01, * p < 0.05).

(I) ECAR profile of LN428/MPG cells treated with either media or media supplemented with 1 mM NR for 24 hr followed by a 1 hr treatment with MNNG. Data are the mean of three independent experiments \pm SD (** p < 0.01, * p < 0.05).

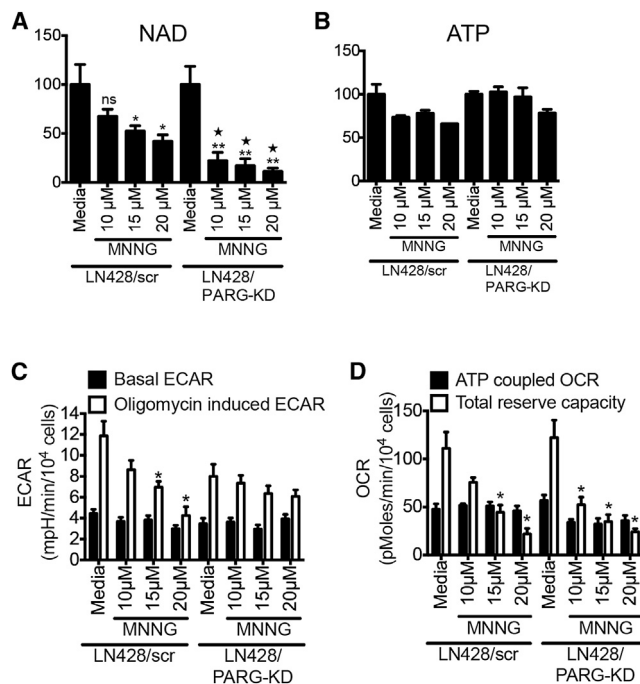


Figure 4. Absence of PARG Rescues Loss of ATP and Glycolytic Defects in LN428 Cells after High-Dose MNNG Treatment

(A and B) Global NAD⁺ (A) and global ATP (B) measured in LN428/scr and LN428/PARG-KD cells after 1 hr exposure to increasing doses of MNNG. Shown is the mean of three independent experiments (ns, nonsignificant; * p < 0.04 compared to media-treated LN428/scr cells; ** p < 0.01 compared to media-treated LN428/PARG-KD cells; * p < 0.005 compared to each respective dose of MNNG in LN428/scr cells).

(C and D) Seahorse measurement of ECAR metabolic profile (C) and OCR metabolic profile (D) of LN428/scr or LN428/PARG-KD cells treated with either media or MNNG (1 hr) at 10 μ M, 15 μ M, and 20 μ M. Shown is the mean of three independent experiments \pm SD (* p < 0.05).

polymers synthesized by ARTD1 hyperactivation, we stably depleted PARG in LN428 cells (Figure S5A). As expected, the absence of PARG elevates the steady-state level of PAR in response to MNNG treatment (Figure S5B). The global NAD⁺ pool was depleted to a greater degree in LN428/PARG-KD cells than in LN428 cells when exposed to increasing concentrations of MNNG but the global ATP pool was not reduced (Figures 4A and 4B). As predicted by the loss of NAD⁺ following MNNG treatment, we observed a dose-dependent decrease of TRC in both the LN428 and LN428/PARG-KD cell lines (Figures 4D and S5C). In line with a role for PARG in the PAR-mediated ATP loss, the oligomycin-induced ECAR is stable in the LN428/PARG-KD cells but decreases in the LN428 cells (Figures 4C and S5D). Together, these data suggest that loss of PARG (LN428/PARG-KD cells) confers resistance to the glycolytic block induced by ARTD1 activation and implicates PARG (via PAR hydrolysis) in the crosstalk between the nucleus and the mitochondria.

PAR Interactome following MNNG-Induced Accumulation of BER Intermediates

Because NAD⁺ biosynthesis inhibition is not sufficient to decrease glycolysis and the block to glycolysis is impacted by

PARG expression, we hypothesized that ARTD1 activation and the subsequent production of PAR might be causing the inhibition of glycolysis. We therefore sought to examine proteins that interact with or are modified by PAR following induction by MNNG treatment. We reasoned that the “PAR interactome” would provide insight into the relationship between ARTD1 activation and the loss of glycolysis. We used a specially designed cell line in which Pol β is disrupted by shRNA-mediated knockdown and re-expressed with its catalytically dead form (5′deoxyribose phosphate, 5′dRP, lyase Pol β mutant K72A). We reasoned that enhanced and persistent BER intermediates and higher activation of ARTD1 in the isogenic cell line LN428/MPG/Pol β -KD/Flag-Pol β (K72) at MNNG doses 20-fold lower than that used in earlier proteome-wide analyses would provide an ideal platform to identify PAR-modified and PAR-interacting proteins resulting from MNNG exposure.

Exposure of LN428/MPG/Pol β -KD/Flag-Pol β (K72) cells to MNNG (5 μ M, 5 min) and isolation of PAR-containing complexes through antibody-based affinity purification was done essentially as described (Gagné et al., 2008, 2012; Figure S6A). Proteins either covalently modified by PAR or those in a multiprotein complex with PAR were identified by liquid-chromatography tandem mass spectrometry (LC-MS/MS) to establish a PAR-interactome in response to MNNG (Figure S6B and Files S1 and S2). As would be expected, the majority of the proteins identified are DNA repair and DNA damage response proteins, but we also found many novel pathways that are significantly overrepresented, including mitochondrial transport and organization, RNA biosynthesis and transcription as well as chromatin assembly (Figures S6B and S6C). Consistent with our findings that ARTD1-activation may have a direct role in altering energy metabolism, we also found a significant number of proteins that reside in the mitochondria and function to synthesize metabolic precursors and energy metabolites (Figures S6B and S6C). These include four proteins involved in glycolysis and ATP metabolism: HK1, the mitochondrial channel proteins voltage-dependent anion channels 1 and 2 (VDAC1 and 2) and the ATP/ADP translocase 2, ANT2 (see Files S1 and S2). For validation, an identical antibody-based affinity-purification workflow was followed by immunoblots for selected proteins to independently confirm the covalently PARylated and PAR-bound protein complexes. Treatment of LN428/MPG/Pol β -KD/Flag-Pol β (K72) cells yielded the expected PAR-bound complexes including ARTD1, XRCC1, DNA-PKcs, and H2B (Figure 5A), as well as DNA ligase III and VDAC1 (Figure S6E). Consistent with the liquid chromatography-tandem mass spectroscopy analysis, we find that some of the validated proteins are either bound to or modified by PAR even in the absence of MNNG treatment.

Loss of Hexokinase 1 Subcellular Localization and Activity due to DNA Damage-Induced ARTD1 Activation

The identification of the HK1/VDAC ATP biosynthesis network in our PAR interactome (Figure S6F) presents a mechanistic link between ARTD1 activation and DNA damage-induced block to glycolysis, providing a direct confirmation of previous bioinformatics analyses, which suggested that HK1 harbors a PAR-binding motif (PBM) (Gagné et al., 2008). As a validation of our proteomic screen, we found that an elevated level of

HK1 was in a complex with PAR upon MNNG treatment (Figure 5B). Reverse IP analysis was used to confirm whether HK1 is modified directly by PAR or is a PAR binding protein. EGFP-tagged HK1 as well as EGFP-tagged XRCC1 or EGFP as a positive and negative control, respectively, were expressed in LN428/MPG cells (Figure 5C). Whereas immunoprecipitation (IP) of EGFP-tagged XRCC1 shows PAR covalent modification (Figure 5C, last lane), neither EGFP nor EGFP-tagged HK1 show PAR modification after immunoblot (Figure 5C, first and middle lanes), supporting the conclusion that the identity of HK1 in our PAR-interactome is more likely the result of an HK1/PAR complex forming via a PBM and not a covalent modification of HK1 by PAR.

The alignment of HK1 with bona fide PAR binding motifs from histones H2A, H2B, H3, H4B (known to encode very strong PBMs), XRCC1 (Pleschke et al., 2000), the mitochondrial protein AIF (Wang et al., 2011; Yu et al., 2002, 2006), the stress signaling protein DEK (Fahrer et al., 2010; Kappes et al., 2008), the experimentally validated PBM within hnRNP-A1 (Gagné et al., 2003; Ji et al., 2013; Ji and Tulin, 2009), and Werner syndrome protein (Popp et al., 2013) supports that HK1 encodes a PBM (Figure 6A). To confirm, we spotted purified BSA, histone H2B and HK1 (0.5, 1, and 2 μ g) on a nitrocellulose membrane and incubated in renaturing buffer containing in vitro synthesized PAR and analyzed by a PAR immunoblot (Figure 6B). As a control experiment, the spotted proteins were incubated in renaturing buffer without PAR (Figure S6G). As expected, BSA does not bind PAR whereas histone H2B presents a strong PAR-binding signal. More importantly, we find that HK1 also binds PAR. However, mutation of three essential amino residues within the HK1-PBM to alanine (Figure 6A) reduces PAR binding to background levels (Figure 6C). Furthermore, a far-western blot with these IP extracts shows no additional PAR binding proteins, indicating the PAR-binding signal in the slot-blot derives from an interaction between PAR and HK1 (Figure S6H). We suggest from these studies that the interaction between HK1 and PAR is not a covalent interaction and that HK1 encodes a PBM that when mutated no longer binds PAR.

We hypothesized that ARTD1 activation and the release of PAR by PARG may alter ATP biosynthesis through PAR binding to HK1. HK1 catalyzes the first step of glycolysis by phosphorylating glucose and generating glucose-6-phosphate. HK1 interacts with the outer mitochondrial membrane protein VDAC and the disruption of its interaction leads to a decrease in the rate of glycolysis (Shoshan-Barmatz and Golan, 2012), presumably due to either an allosteric effect or a decrease in the availability of VDAC transported ATP. To depict HK1 subcellular localization, we expressed HK1 in the LN428/MPG cells as a fusion with EGFP. Under normal conditions, HK1 is localized on the mitochondria and colocalized with the mitochondrial protein Tom20 (Figures 6D and S6I). However, after MNNG treatment, localization of HK1 is also cytoplasmic (Figure 6D). In a parallel evaluation, we characterized the localization of HK1 by a biochemical analysis. In untreated cells, very little HK1 is localized to the cytosol (Figure 6E). However, MNNG treatment induces a significant increase in cytosolic HK1 relocalization (Figure 6E, upper) with little to no observed cytosolic HK1 relocalization in LN428 cells (Figure 6E, lower; Figure S1D).

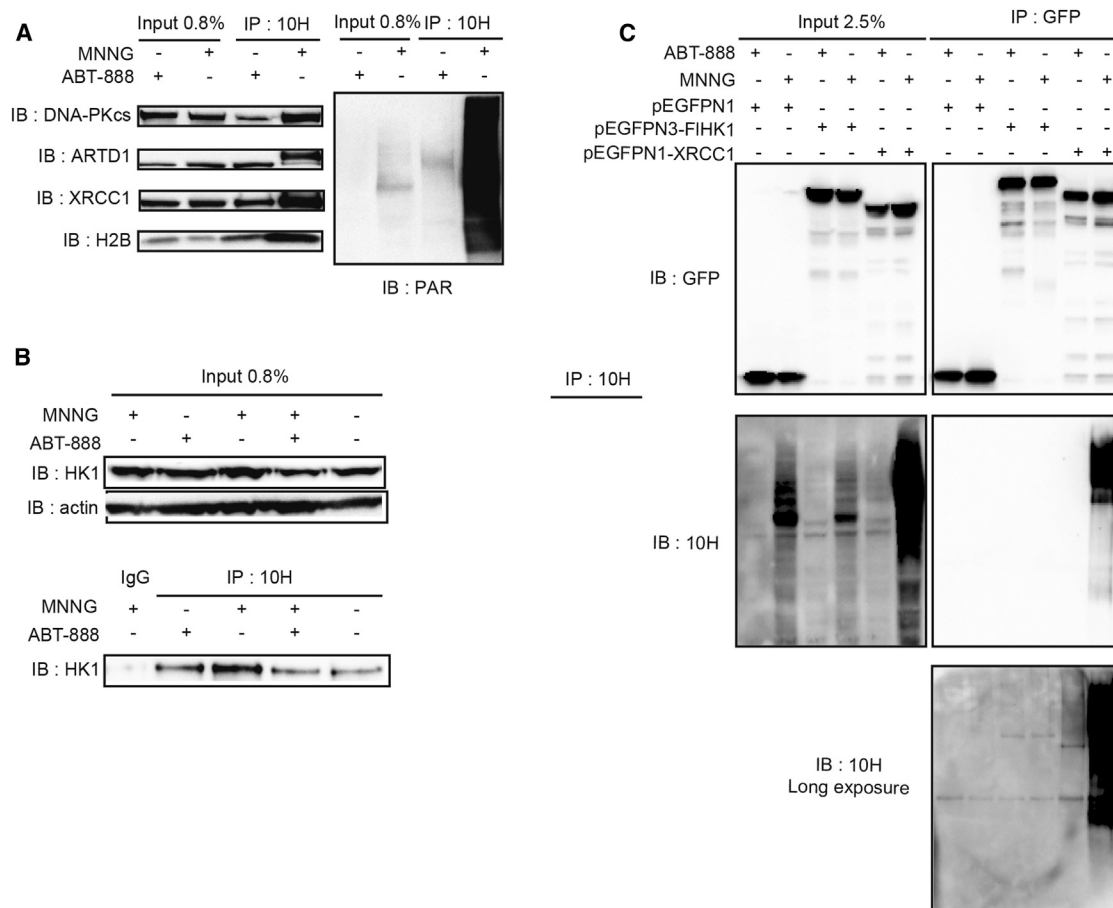


Figure 5. Affinity-Purification and Analysis of PAR-Containing Complexes

(A) Validation by IP/immunoblot of DNA-PKcs, ARTD1, XRCC1, and H2B identified in the mass spectrometry analysis. Left: IP with the anti-PAR Ab 10H and immunoblot with the indicated antibodies. Right: immunoblot for PAR after IP with the anti-PAR (10H) Ab.

(B) Validation by IP/immunoblot of HK1 enzyme identified in the mass spectrometry analysis as described in (A).

(C) Upper: the GFP immunoblot on inputs and IP samples after pull-down of GFP-tagged proteins with GFP-Trap. Cells are treated either with the ARTD1 inhibitor ABT-888 (10 μ M; 30 min) or with MNNG (5 μ M; 5 min). Lower: PAR immunoblot on inputs and IP samples. PAR immunoblot on IP samples is shown as short and long exposures.

Furthermore, we observed that the MNNG-induced cytosolic HK1 relocalization is suppressed by pretreatment with the ARTD1 inhibitor ABT-888 or by mutation of the HK1 PAR-binding motif, HK1/PBM (Figure S6J). Moreover, HK1 activity was found to be 3-fold lower in LN428/MPG cells treated with MNNG than in untreated cells and HK1 activity was restored by ARTD1 inhibition or knockdown (Figure 6F), indicating a role of ARTD1 hyperactivation in HK1 inactivation. It is noteworthy that even a 3-fold higher dose of MNNG does not lead to HK1 activity alteration in LN428/ARTD1-KD/MPG cells (Figure 6F). Interestingly, MNNG treatment of LN428 cells leads to a slight HK1 activity decrease yet not to the same extent as in LN428/MPG cells (Figure 6G, upper) and the knockdown of PARG partially rescues these defects (Figure 6G, lower). Furthermore, we measured HK1 activity after incubation of purified HK1 with 50 or 100 pmol of in vitro synthesized PAR (Figure 6H) and observed a progressive decrease in HK1 activity with increasing doses of PAR, demonstrating a direct role of ARTD1 in HK1 inactivation.

Together, these results support our hypothesis that HK1 is a direct target of ARTD1 activation. Once activated, ARTD1-induced PAR is released from the nucleus via PARG activity. In turn, the DNA damage-induced loss of ATP biosynthesis can be mediated by release of HK1 from the mitochondrial membrane into the cytosol and PAR-mediated inhibition of HK1 activity. In total, the result is a block to glycolysis.

DISCUSSION

While cell death induced by ARTD1 hyperactivation is well documented, the precise mechanism underlying this observed phenotype remains unresolved and is still a matter of debate. In this study, we demonstrate that ARTD1-induced NAD⁺ depletion is not the only factor to mediate metabolic collapse and induce cell death. On the contrary, we show an unambiguous, direct role of ARTD1, through the induction of PAR and the inhibition of hexokinase 1 activity, clarifying the mechanism of

ARTD1-directed metabolic collapse. Most importantly, our study brings insight into the importance of the crosstalk between nuclear ARTD1 activity and other cell compartments, particularly the mitochondria (Andrabi et al., 2008).

It is well established that PAR produced after DNA damage is a key intermediate that triggers a cascade of events leading to cell death. One of these events, initially postulated “PARP-assisted cell suicide,” attempts to explain the observed cell death by speculating that NAD⁺ depletion caused by ARTD1 hyperactivity causes a shut-down of NAD⁺/NADH-dependent metabolic pathways followed by ATP depletion and the onset of necrosis (Berger et al., 1983; Ha and Snyder, 1999; Vyas et al., 2013). In line with this theory, we report a significant energy defect in DNA damaged cells due to ARTD1 hyperactivation. We have used two state-of-the-art techniques in live cells to show that incomplete repair of MNNG-induced DNA damage causes a massive increase in ARTD1 activity and a subsequent decline in ATP supplied from both oxidative phosphorylation and glycolysis. Whereas others have reported a decrease of the mitochondrial membrane potential (Juarez-Salinas et al., 1979; Leung et al., 2012), we have been able to measure a loss of total mitochondrial reserve capacity (TRC), a mitochondrial defect, which evaded detection in past studies using mitochondrial extracts.

Glycolysis and the TCA cycle are the two main NAD⁺-consuming pathways in cells as well as the major NADH providers to the respiratory chain that produce ATP. Although the shutdown of these pathways by ARTD1 hyperactivation-mediated NAD⁺ loss could explain the respiratory defects in cells exposed to DNA damage, loss of NAD⁺ production by direct enzymatic inhibition of NAMPT using FK866 did not cause a decrease in glycolysis. Because these data are in contrast to current models (Alano et al., 2010), we demonstrate that the glycolytic block upon MNNG treatment is not a mere consequence of NAD⁺ loss. Rather, we speculate that ARTD1 hyperactivation has a direct effect on glycolysis via PAR. This hypothesis is further supported by the lack of a glycolysis rate rescue after NAD⁺ synthesis precursor pretreatment, whereas ARTD1 inhibition by ABT-888 or BMN-673 as well as ARTD1 knockdown, restores glycolysis.

Consistent with our hypothesis that ARTD1 directly affects glycolysis, we identified the glycolytic protein HK1, the enzyme responsible for the first step of glycolysis, as a potential PAR binding protein by mass spectrometry. We find that although HK1 is not covalently modified by ARTD1, HK1 binds PAR through a PBM earlier identified by mass spectrometry analysis (Gagné et al., 2008). HK1 is one of the three major isoenzymes of the hexokinase family. HK1 is mainly associated with the outer mitochondrial membrane through an interaction with the channel protein VDAC, also identified in our PAR binding protein mass spectrometry analysis (see Files S1 and S2; Jun et al., 2012; Wilson, 2003). This physical interaction couples cytosolic glycolysis to mitochondrial oxidative phosphorylation by which the cells produce most of their ATP and potentially links ARTD1 activity and PAR to the metabolic events in the mitochondria. Indeed, a previous study has demonstrated that during ischemic renal injury, ARTD1 can poly(ADP-ribosyl)ate and inhibit glyceraldehyde-3-phosphate-dehydrogenase (GAPDH), the enzyme responsible for the catalysis of the second step of glycolysis (Devalaraja-Narashimha and Padanilam, 2009). We also

observed that GAPDH is bound or modified by PAR but at an extremely low level, suggesting that the PAR-interactome we have identified may be selective for a cellular response to BER intermediates (see Files S1 and S2). Our PAR binding protein mass spectrometry analysis also identified three enzymes involved in the Krebs cycle (succinate dehydrogenase, alpha-ketoglutarate dehydrogenase, and pyruvate dehydrogenase), suggesting a possible role of ARTD1 in the regulation of these enzyme activities after DNA damage. Consistent with this idea, we found that although NR pretreatment is able to partly rescue the global NAD⁺ pool after MNNG treatment at low doses, both the TRC and ECAR were still affected (Figures S4G and S4H). Ying and colleagues previously demonstrated that treatment of murine astrocytes after MNNG with TCA cycle intermediates partly rescued cell death (Ying et al., 2002). These results confirm our observation that ARTD1 hyperactivation is directly involved in the inhibition of glycolysis after MNNG treatment and does not exclude the possible involvement of ARTD1 in the control of the TCA cycle enzymes.

MNNG-induced ARTD1 hyperactivation could negatively affect glycolysis by creating excess PAR able to migrate into the cytosol and bind to HK1 and thus inhibit its enzyme activity. In support of this hypothesis, we find that the ECAR values of LN428/PARG-KD cells are more resistant to MNNG than LN428 cells. In addition, we observe a decrease in HK1 activity in LN428/MPG cell lysates after MNNG treatment that is rescued by ARTD1 inhibition, and more importantly a direct effect of HK1 activity upon *in vitro* incubation with PAR. These two key results constitute strong evidence for a role of ARTD1 in controlling HK1 activity under cellular stress. Interestingly, some studies correlate HK1 subcellular localization and activity. It has been demonstrated that the release of HK1 can affect its activity (Saraiva et al., 2010). HK1 release from the mitochondria may also be responsible for a decrease in the mitochondrial membrane potential and can promote tumor necrosis factor-induced apoptosis in HeLa cells (Ullu et al., 2002). Intriguingly, we find a mobilization of HK1 from the mitochondria to the cytosol after MNNG treatment in LN428/MPG cells, consistent with the observed reduction of HK1 activity.

These findings suggest a working model in which ARTD1 hyperactivation leads to inhibition of HK1 and mislocalization of HK1 from the outer mitochondrial membrane, leading to a reduction in cellular glycolysis and depletion in cellular ATP pools. This effect of ARTD1 activity coupled with NAD⁺ depletion might explain the cell sensitivity in response to DNA alkylation damage and the resulting ARTD1 activation that is induced due to unrepaired DNA strand breaks and BER intermediates. PAR could affect HK1 activity in two nonmutually exclusive ways. First, PAR binding to HK1 could cause a decrease in its affinity to VDAC causing its migration into the cytoplasm. Second, PAR binding could allosterically affect HK1 activity. Data presented here support both mechanisms. Furthermore, high-resolution crystal structures indicate that the putative PBM of HK1 is located in an accessible surface area that overlaps with a helix in its N-terminal domain (Rosano, 2011). This helical domain is involved both in the binding of ATP and in the interaction of HK1 with the mitochondrial protein channel VDAC1, making both scenarios plausible.

Another group reported that mouse cortical neurons treated with high-dose MNNG undergo ARTD1-dependent energy depletion that is mediated by glycolysis inhibition (Andrabi et al., 2014). The authors hypothesize that PAR-induced release of AIF could be responsible for the ARTD1 activation-induced decrease in HK1 activity via the loss of an interaction between both proteins. Further to this point, we demonstrate the ARTD1 activation-dependent release of HK1 into the cytosol, previously suggested as being responsible for HK1 inhibition (Saraiva et al., 2010). In addition to demonstrating the PAR-dependent release of HK1, we also show that the HK1-PBM is required for ARTD1 activation-induced inhibition of HK1, implicating binding of PAR to HK1 as a requisite event. Future studies will reveal the role of PAR in the regulation of HK1 and the contribution of this interaction to the loss of glycolysis, mitochondrial dysfunction, and the onset of parthanatos in response to genotoxin exposure.

In summary, we propose a model in which DNA repair intermediates induce ARTD1 hyperactivation. In turn, the resulting PAR synthesis leads to a release of PAR units in the cytoplasm, which upon binding to HK1 causes the decrease of its activity and/or its dissociation from VDAC, leading to its release into the cytoplasm and a subsequent decrease in its activity. Such a model, in which PAR would be required to migrate from the nucleus to the mitochondria, is consistent with a role for both PARG and the ADP-ribosylhydrolase like 2 protein (ARH3) regulating such a response, as recently suggested (Mashimo et al., 2013). Data presented in this study therefore provide a molecular mechanism linking DNA damage induced ARTD1 hyperactivation to cell death through the direct inhibition of glycolysis by diminishing HK1 activity. These data are in contrast to the previously proposed “secondary shutdown” of the glycolytic pathway by ARTD1-mediated NAD⁺ depletion. Our findings have wide-ranging implications not only for the fields of DNA repair, BER, and chemotherapy, but also for diseases in which ARTD1 activation plays a prominent role, such as ischemic injury after stroke or myocardial infarction, traumatic brain injury, Parkinson disease, and septic shock.

EXPERIMENTAL PROCEDURES

More details on the experimental procedures are provided in the [Supplemental Experimental Procedures](#) section.

Cell Culture

The cell line LN428 has been established as previously reported and LN428/MPG cells were prepared and cultured as described (Tang et al., 2010). LN428/ARTD1-KD/copGFP, LN428/ARTD1-KD/MPG-copGFP, LN428/MPG/PARG-KD, and LN428/PARG-KD cells are stable cell lines developed by lentiviral transduction, essentially as described (Goellner et al., 2011; Svalar et al., 2012; Tang et al., 2010).

Cell Cytotoxicity

MNNG- and FK866-induced cytotoxicity was determined by an MTS assay and a modified MTT assay as described previously (Tang et al., 2010).

Hexokinase Activity

Hexokinase activity of purified protein and from cell lysates was measured using the Hexokinase Colorimetric Assay (BioVision).

Global NAD⁺ and ATP Measurements

Global NAD⁺ and ATP pools were measured using the EnzyChrom NAD⁺/NADH Assay kit (BioAssay Systems) and the ATP lite assay kit (Perkin-Elmer), respectively.

Subcellular ATP Analysis

Subcellular ATP levels were evaluated by fluorescence resonance energy transfer (FRET) using the ATeam probes composed of mVenus and mseCFP linked to the ϵ subunit of *Bacillus subtilis* F₀F₁-ATP synthase (Imamura et al., 2009a) and targeted to the three different cell compartments.

Metabolic Flux Measurement

The OCRs and ECARs were measured using the Seahorse Extracellular Flux Analyzer (Seahorse Bioscience), essentially as described (Furda et al., 2012; Qian and Van Houten, 2010; Varum et al., 2011).

PAR Dot Blot and Far Western Blot

PAR was synthesized in vitro as previously described (Amé et al., 2009) or obtained in purified form from Trevigen (#4336-100-01). Purified proteins (BSA, H2B or HK1; 0.5, 1 or 2 μ g) were spotted on a nitrocellulose membrane and incubated in renaturing buffer containing PAR polymers. The presence of bound PAR was then detected by immunoblot using the 10H anti-PAR antibody. For the far western blot, GFP-tagged proteins were expressed in LN428 cells, isolated using GFP-Trap (Chromotek) beads, and resolved by SDS-PAGE followed by transfer to a nitrocellulose membrane. The membrane was incubated in renaturing buffer as described above and the PAR signal was detected using 10H antibody conjugated to biotin, followed by incubation with streptavidin-HRP.

Immunoprecipitation

LN428/MPG/Pol β -KD/FLAG-Pol β (K72A) or LN428/MPG cells were seeded onto 15 mm dishes and grown to 80%–90% confluence. Cells were either treated with ABT-888 (10 μ M, 1 hr) and/or with MNNG (5 μ M, 5 min) and then cell lysates were prepared for immunoprecipitation with either the 10H anti-PAR Ab or the GFP-Trap (Chromotek).

Immunofluorescence and Confocal Microscopy

Cells were seeded on glass coverslips for 24 hr before MNNG treatment during the time indicated preceded by PJ34 (or vehicle) pretreatment. The immunodetection of PAR was performed as previously described (Amé et al., 2009). For immunodetection of HK1-GFP, cells were modified to express HK1-GFP by transfection with pEGFP-N3-FLHK1 (AddGene) using the transfection reagent JetPrime (VWR) 24 hr prior to the cell treatment and fixation for immunofluorescence. To depict the mitochondria, an antibody against the membrane protein Tom20 has been used (SantaCruz).

Mass Spectrometry

After immunoprecipitation of the PAR binding complexes, mass spectrometry analyses were performed on a TripleTOF 5600 mass spectrometer fitted with a nanospray III ion source (ABSciex) and coupled to an Agilent 1200 HPLC (extensive details are reported in the [Supplemental Experimental Procedures](#)).

SUPPLEMENTAL INFORMATION

Supplemental Information includes Supplemental Experimental Procedures, six figures, Excel and Scaffold database files, and three movies and can be found with this article online at <http://dx.doi.org/10.1016/j.celrep.2014.08.036>.

(5 μ M, hatched light-gray bar and 15 μ M, hatched dark-gray bar). ns, nonsignificant compared to LN428/MPG cells untreated; *p < 0.05 compared to MNNG treated LN428/MPG cells. LN428 and LN428/PARG-KD cells were treated with 5 μ M, 10 μ M, and 20 μ M MNNG (1 hr). (H) PAR binding leads to HK1 activity decrease in vitro. HK1 activity is measured in vitro 20 min after incubation of 0.25 μ g of HK1 with in vitro synthesized PAR (50 pmol or 100 pmol), using an HK1 colorimetric assay. Data are the mean of two independent experiments \pm SD.

AUTHOR CONTRIBUTIONS

E.F., E.G., J.P.G., G.G.P., and R.W.S. designed the experiments; E.F., E.G., Z.Y., and J.P.G. performed the experiments; E.F., E.G., J.P.G., G.G.P., D.W., M.M., G.R., and R.W.S. analyzed data; P.R., J.L., T.F., M.B.M., and M.M. contributed new reagents/analytic tools; E.F., E.G., and R.W.S. wrote the paper with comments by Z.Y., D.W., P.R., G.R., J.P.G., G.G.P., M.M., and B.V.H.

ACKNOWLEDGMENTS

This work was supported by grants from NIH (CA148629, GM087798, ES019498, ES021116, GM099213, and CA148629-04S1) to R.W.S., from the Canadian Institutes of Health Research (MOP-178013, MOP-209278) to G.G.P., and from PA CURE to B.V.H. Support for the synthetic chemistry conducted by P.R. was provided by the John King Laboratory Funds. Support was also provided by the University of Pittsburgh Department of Pharmacology & Chemical Biology through a Pharmacology Fellowship to E.M.G. G.G.P. holds a Tier1 Canada Chair in Proteomics. B.V.H. holds the Richard M. Cyert Chair as Professor of Molecular Oncology. Support for the UPCI Lentiviral (Vector Core) Facility and the UPCI Cell and Tissue Imaging Facility was provided in part by the Cancer Center Support Grant from the NIH (P30CA047904). RWS is a scientific consultant for Trevigen, Inc.

Received: February 18, 2014

Revised: August 11, 2014

Accepted: August 19, 2014

Published: September 11, 2014

REFERENCES

- Alano, C.C., Ying, W., and Swanson, R.A. (2004). Poly(ADP-ribose) polymerase-1-mediated cell death in astrocytes requires NAD⁺ depletion and mitochondrial permeability transition. *J. Biol. Chem.* *279*, 18895–18902.
- Alano, C.C., Garnier, P., Ying, W., Higashi, Y., Kauppinen, T.M., and Swanson, R.A. (2010). NAD⁺ depletion is necessary and sufficient for poly(ADP-ribose) polymerase-1-mediated neuronal death. *J. Neurosci.* *30*, 2967–2978.
- Almeida, K.H., and Sobol, R.W. (2007). A unified view of base excision repair: lesion-dependent protein complexes regulated by post-translational modification. *DNA Repair (Amst.)* *6*, 695–711.
- Amé, J.C., Hakmé, A., Quenet, D., Fouquerel, E., Dantzer, F., and Schreiber, V. (2009). Detection of the nuclear poly(ADP-ribose)-metabolizing enzymes and activities in response to DNA damage. *Methods Mol. Biol.* *464*, 267–283.
- Andrabi, S.A., Kim, N.S., Yu, S.W., Wang, H., Koh, D.W., Sasaki, M., Klaus, J.A., Otsuka, T., Zhang, Z., Koehler, R.C., et al. (2006). Poly(ADP-ribose) (PAR) polymer is a death signal. *Proc. Natl. Acad. Sci. USA* *103*, 18308–18313.
- Andrabi, S.A., Dawson, T.M., and Dawson, V.L. (2008). Mitochondrial and nuclear cross talk in cell death: parthanatos. *Ann. N Y Acad. Sci.* *1147*, 233–241.
- Andrabi, S.A., Umanah, G.K., Chang, C., Stevens, D.A., Karuppagounder, S.S., Gagné, J.P., Poirier, G.G., Dawson, V.L., and Dawson, T.M. (2014). Poly(ADP-ribose) polymerase-dependent energy depletion occurs through inhibition of glycolysis. *Proc. Natl. Acad. Sci. USA* *111*, 10209–10214.
- Berger, N.A. (1985). Poly(ADP-ribose) in the cellular response to DNA damage. *Radiat. Res.* *101*, 4–15.
- Berger, N.A., Sims, J.L., Catino, D.M., and Berger, S.J. (1983). Poly(ADP-ribose) polymerase mediates the suicide response to massive DNA damage: studies in normal and DNA-repair defective cells. *Int. Symp. Princess Takamatsu Cancer Res. Fund* *13*, 219–226.
- Burns, N., and Gold, B. (2007). The effect of 3-methyladenine DNA glycosylase-mediated DNA repair on the induction of toxicity and diabetes by the beta-cell toxicant streptozotocin. *Toxicol. Sci.* *95*, 391–400.
- Calvo, J.A., Moroski-Erkul, C.A., Lake, A., Eichinger, L.W., Shah, D., Jhun, I., Limsirichai, P., Bronson, R.T., Christiani, D.C., Meira, L.B., and Samson, L.D. (2013). Aag DNA glycosylase promotes alkylation-induced tissue damage mediated by Parp1. *PLoS Genet.* *9*, e1003413.
- Cipriani, G., Rapizzi, E., Vannacci, A., Rizzuto, R., Moroni, F., and Chiarugi, A. (2005). Nuclear poly(ADP-ribose) polymerase-1 rapidly triggers mitochondrial dysfunction. *J. Biol. Chem.* *280*, 17227–17234.
- De Vos, M., Schreiber, V., and Dantzer, F. (2012). The diverse roles and clinical relevance of PARPs in DNA damage repair: current state of the art. *Biochem. Pharmacol.* *84*, 137–146.
- Devalaraja-Narashimha, K., and Padanilam, B.J. (2009). PARP-1 inhibits glycolysis in ischemic kidneys. *J. Am. Soc. Nephrol.* *20*, 95–103.
- Eliasson, M.J., Sampei, K., Mandir, A.S., Hurn, P.D., Traystman, R.J., Bao, J., Pieper, A., Wang, Z.Q., Dawson, T.M., Snyder, S.H., and Dawson, V.L. (1997). Poly(ADP-ribose) polymerase gene disruption renders mice resistant to cerebral ischemia. *Nat. Med.* *3*, 1089–1095.
- Endres, M., Wang, Z.Q., Namura, S., Waeber, C., and Moskowitz, M.A. (1997). Ischemic brain injury is mediated by the activation of poly(ADP-ribose) polymerase. *J. Cereb. Blood Flow Metab.* *17*, 1143–1151.
- Fahrer, J., Popp, O., Malanga, M., Beneke, S., Markovitz, D.M., Ferrando-May, E., Bürkle, A., and Kappes, F. (2010). High-affinity interaction of poly(ADP-ribose) and the human DEK oncoprotein depends upon chain length. *Biochemistry* *49*, 7119–7130.
- Fu, D., Calvo, J.A., and Samson, L.D. (2012). Balancing repair and tolerance of DNA damage caused by alkylating agents. *Nat. Rev. Cancer* *12*, 104–120.
- Furda, A.M., Marrangoni, A.M., Lokshin, A., and Van Houten, B. (2012). Oxidants and not alkylating agents induce rapid mtDNA loss and mitochondrial dysfunction. *DNA Repair (Amst.)* *11*, 684–692.
- Gagné, J.P., Hunter, J.M., Labrecque, B., Chabot, B., and Poirier, G.G. (2003). A proteomic approach to the identification of heterogeneous nuclear ribonucleoproteins as a new family of poly(ADP-ribose)-binding proteins. *Biochem. J.* *371*, 331–340.
- Gagné, J.P., Isabelle, M., Lo, K.S., Bourassa, S., Hendzel, M.J., Dawson, V.L., Dawson, T.M., and Poirier, G.G. (2008). Proteome-wide identification of poly(ADP-ribose) binding proteins and poly(ADP-ribose)-associated protein complexes. *Nucleic Acids Res.* *36*, 6959–6976.
- Gagné, J.P., Pic, E., Isabelle, M., Krietsch, J., Ethier, C., Paquet, E., Kelly, I., Boutin, M., Moon, K.M., Foster, L.J., and Poirier, G.G. (2012). Quantitative proteomics profiling of the poly(ADP-ribose)-related response to genotoxic stress. *Nucleic Acids Res.* *40*, 7788–7805.
- Goellner, E.M., Grimme, B., Brown, A.R., Lin, Y.C., Wang, X.H., Sugrue, K.F., Mitchell, L., Trivedi, R.N., Tang, J.B., and Sobol, R.W. (2011). Overcoming temozolomide resistance in glioblastoma via dual inhibition of NAD⁺ biosynthesis and base excision repair. *Cancer Res.* *71*, 2308–2317.
- Gottipati, P., Vischioni, B., Schultz, N., Solomons, J., Bryant, H.E., Djureinovic, T., Issaeva, N., Sleeth, K., Sharma, R.A., and Helleday, T. (2010). Poly(ADP-ribose) polymerase is hyperactivated in homologous recombination-defective cells. *Cancer Res.* *70*, 5389–5398.
- Ha, H.C., and Snyder, S.H. (1999). Poly(ADP-ribose) polymerase is a mediator of necrotic cell death by ATP depletion. *Proc. Natl. Acad. Sci. USA* *96*, 13978–13982.
- Hasmann, M., and Schemainda, I. (2003). FK866, a highly specific noncompetitive inhibitor of nicotinamide phosphoribosyltransferase, represents a novel mechanism for induction of tumor cell apoptosis. *Cancer Res.* *63*, 7436–7442.
- Hassa, P.O., Haenni, S.S., Elser, M., and Hottiger, M.O. (2006). Nuclear ADP-ribosylation reactions in mammalian cells: where are we today and where are we going? *Microbiol. Mol. Biol. Rev.* *70*, 789–829.
- Hottiger, M.O., Hassa, P.O., Lüscher, B., Schüler, H., and Koch-Nolte, F. (2010). Toward a unified nomenclature for mammalian ADP-ribosyltransferases. *Trends Biochem. Sci.* *35*, 208–219.
- Imamura, H., Nhat, K.P., Togawa, H., Saito, K., Iino, R., Kato-Yamada, Y., Nagai, T., and Noji, H. (2009b). Visualization of ATP levels inside single living cells with fluorescence resonance energy transfer-based genetically encoded indicators. *Proc. Natl. Acad. Sci. USA* *106*, 15651–15656.
- Jacobson, M.K., Levi, V., Juarez-Salinas, H., Barton, R.A., and Jacobson, E.L. (1980). Effect of carcinogenic N-alkyl-N-nitroso compounds on nicotinamide adenine dinucleotide metabolism. *Cancer Res.* *40*, 1797–1802.

- Ji, Y., and Tulin, A.V. (2009). Poly(ADP-ribose)ylation of heterogeneous nuclear ribonucleoproteins modulates splicing. *Nucleic Acids Res.* *37*, 3501–3513.
- Ji, Y., Jarnik, M., and Tulin, A.V. (2013). Poly(ADP-ribose) glycohydrolase and poly(ADP-ribose)-interacting protein Hrp38 regulate pattern formation during *Drosophila* eye development. *Gene* *526*, 187–194.
- Juarez-Salinas, H., Sims, J.L., and Jacobson, M.K. (1979). Poly(ADP-ribose) levels in carcinogen-treated cells. *Nature* *282*, 740–741.
- Jun, B.H., Kang, H., Lee, Y.S., and Jeong, D.H. (2012). Fluorescence-based multiplex protein detection using optically encoded microbeads. *Molecules* *17*, 2474–2490.
- Kappes, F., Fahrer, J., Khodadoust, M.S., Tabbert, A., Strasser, C., Morvaknin, N., Moreno-Villanueva, M., Bürkle, A., Markovitz, D.M., and Ferrando-May, E. (2008). DEK is a poly(ADP-ribose) acceptor in apoptosis and mediates resistance to genotoxic stress. *Mol. Cell. Biol.* *28*, 3245–3257.
- Langelier, M.F., Planck, J.L., Roy, S., and Pascal, J.M. (2012). Structural basis for DNA damage-dependent poly(ADP-ribose)ylation by human PARP-1. *Science* *336*, 728–732.
- Leung, A., Todorova, T., Ando, Y., and Chang, P. (2012). Poly(ADP-ribose) regulates post-transcriptional gene regulation in the cytoplasm. *RNA Biol.* *9*, 542–548.
- Mashimo, M., Kato, J., and Moss, J. (2013). ADP-ribosyl-acceptor hydrolase 3 regulates poly(ADP-ribose) degradation and cell death during oxidative stress. *Proc. Natl. Acad. Sci. USA* *110*, 18964–18969.
- Masson, M., Niedergang, C., Schreiber, V., Muller, S., Menissier-de Murcia, J., and de Murcia, G. (1998). XRCC1 is specifically associated with poly(ADP-ribose) polymerase and negatively regulates its activity following DNA damage. *Mol. Cell. Biol.* *18*, 3563–3571.
- Masutani, M., Suzuki, H., Kamada, N., Watanabe, M., Ueda, O., Nozaki, T., Jishage, K., Watanabe, T., Sugimoto, T., Nakagama, H., et al. (1999). Poly(ADP-ribose) polymerase gene disruption conferred mice resistant to streptozotocin-induced diabetes. *Proc. Natl. Acad. Sci. USA* *96*, 2301–2304.
- Pieper, A.A., Brat, D.J., Krug, D.K., Watkins, C.C., Gupta, A., Blackshaw, S., Verma, A., Wang, Z.Q., and Snyder, S.H. (1999). Poly(ADP-ribose) polymerase-deficient mice are protected from streptozotocin-induced diabetes. *Proc. Natl. Acad. Sci. USA* *96*, 3059–3064.
- Pieper, A.A., Walles, T., Wei, G., Clements, E.E., Verma, A., Snyder, S.H., and Zweier, J.L. (2000). Myocardial postischemic injury is reduced by polyADP-ribose polymerase-1 gene disruption. *Mol. Med.* *6*, 271–282.
- Pleschke, J.M., Kleczkowska, H.E., Strohm, M., and Althaus, F.R. (2000). Poly(ADP-ribose) binds to specific domains in DNA damage checkpoint proteins. *J. Biol. Chem.* *275*, 40974–40980.
- Popp, O., Veith, S., Fahrer, J., Bohr, V.A., Bürkle, A., and Mangerich, A. (2013). Site-specific noncovalent interaction of the biopolymer poly(ADP-ribose) with the Werner syndrome protein regulates protein functions. *ACS Chem. Biol.* *8*, 179–188.
- Qian, W., and Van Houten, B. (2010). Alterations in bioenergetics due to changes in mitochondrial DNA copy number. *Methods* *51*, 452–457.
- Rosano, C. (2011). Molecular model of hexokinase binding to the outer mitochondrial membrane porin (VDAC1): Implication for the design of new cancer therapies. *Mitochondrion* *11*, 513–519.
- Saraiva, L.M., Seixas da Silva, G.S., Galina, A., da-Silva, W.S., Klein, W.L., Ferreira, S.T., and De Felice, F.G. (2010). Amyloid- β triggers the release of neuronal hexokinase 1 from mitochondria. *PLoS ONE* *5*, e15230.
- Schreiber, V., Dantzer, F., Ame, J.C., and de Murcia, G. (2006). Poly(ADP-ribose): novel functions for an old molecule. *Nat. Rev. Mol. Cell Biol.* *7*, 517–528.
- Shoshan-Barmatz, V., and Golan, M. (2012). Mitochondrial VDAC1: function in cell life and death and a target for cancer therapy. *Curr. Med. Chem.* *19*, 714–735.
- Svilar, D., Goellner, E.M., Almeida, K.H., and Sobol, R.W. (2011). Base excision repair and lesion-dependent subpathways for repair of oxidative DNA damage. *Antioxid. Redox Signal.* *14*, 2491–2507.
- Svilar, D., Dyavaiah, M., Brown, A.R., Tang, J.B., Li, J., McDonald, P.R., Shun, T.Y., Braganza, A., Wang, X.H., Maniar, S., et al. (2012). Alkylation sensitivity screens reveal a conserved cross-species functionome. *Mol. Cancer Res.* *10*, 1580–1596.
- Tang, J.B., Goellner, E.M., Wang, X.H., Trivedi, R.N., St Croix, C.M., Jelezcova, E., Svilar, D., Brown, A.R., and Sobol, R.W. (2010). Bioenergetic metabolites regulate base excision repair-dependent cell death in response to DNA damage. *Mol. Cancer Res.* *8*, 67–79.
- Ullu, E., Djikeng, A., Shi, H., and Tschudi, C. (2002). RNA interference: advances and questions. *Philos. Trans. R. Soc. Lond. B Biol. Sci.* *357*, 65–70.
- Varum, S., Rodrigues, A.S., Moura, M.B., Momcilovic, O., Easley, C.A., 4th, Ramalho-Santos, J., Van Houten, B., and Schatten, G. (2011). Energy metabolism in human pluripotent stem cells and their differentiated counterparts. *PLoS ONE* *6*, e20914.
- Vyas, S., Chesaroni-Cataldo, M., Todorova, T., Huang, Y.H., and Chang, P. (2013). A systematic analysis of the PARP protein family identifies new functions critical for cell physiology. *Nat. Commun.* *4*, 2240.
- Wang, Y., Kim, N.S., Haince, J.F., Kang, H.C., David, K.K., Andrabi, S.A., Poirier, G.G., Dawson, V.L., and Dawson, T.M. (2011). Poly(ADP-ribose) (PAR) binding to apoptosis-inducing factor is critical for PAR polymerase-1-dependent cell death (parthanatos). *Sci. Signal.* *4*, ra20.
- Wilson, J.E. (2003). Isozymes of mammalian hexokinase: structure, subcellular localization and metabolic function. *J. Exp. Biol.* *206*, 2049–2057.
- Ying, W., Chen, Y., Alano, C.C., and Swanson, R.A. (2002). Tricarboxylic acid cycle substrates prevent PARP-mediated death of neurons and astrocytes. *J. Cereb. Blood Flow Metab.* *22*, 774–779.
- Ying, W., Garnier, P., and Swanson, R.A. (2003). NAD⁺ repletion prevents PARP-1-induced glycolytic blockade and cell death in cultured mouse astrocytes. *Biochem. Biophys. Res. Commun.* *308*, 809–813.
- Yu, S.W., Wang, H., Poitras, M.F., Coombs, C., Bowers, W.J., Federoff, H.J., Poirier, G.G., Dawson, T.M., and Dawson, V.L. (2002). Mediation of poly(ADP-ribose) polymerase-1-dependent cell death by apoptosis-inducing factor. *Science* *297*, 259–263.
- Yu, S.W., Andrabi, S.A., Wang, H., Kim, N.S., Poirier, G.G., Dawson, T.M., and Dawson, V.L. (2006). Apoptosis-inducing factor mediates poly(ADP-ribose) (PAR) polymer-induced cell death. *Proc. Natl. Acad. Sci. USA* *103*, 18314–18319.
- Zong, W.X., Ditsworth, D., Bauer, D.E., Wang, Z.Q., and Thompson, C.B. (2004). Alkylating DNA damage stimulates a regulated form of necrotic cell death. *Genes Dev.* *18*, 1272–1282.